APPLICATION

Optimization design and experimental research of magnetic pulse welding system based on uniform pressure electromagnetic actuator

Hang Zhang[1] · Ning Liu[1] · Xiaoxiang Li[1] · Qingjian Wang[1] · Hongfa Ding[1]

Abstract

The magnetic pulse welding method based on uniform pressure electromagnetic actuator can provide a larger area of uniform pressure, which is helpful to increase the welding area, and can be used in some applications where a larger welding area is required. By reasonably optimizing the structural parameters of the magnetic pulse welding device, the size and spatial distribution of magnetic field and eddy current in the welding process can be effectively controlled, and the collision speed of plates can be increased, so as to improve the quality of welded joints. In view of this, this paper proposes an optimal design method for the uniform pressure welding magnet device with the optimization objective of maximizing the magnetic pressure. Then, magnet devices with different structural sizes were developed, and a uniform pressure welding experimental platform was built to realize the high-quality welding of AA1060 aluminum plate and SS304 stainless steel plate both with a thickness of 1 mm under different welding areas, and effective improvement methods are put forward to solve the problems of thinning and tearing of workpiece at chamfer and arc ablation of contact surface in uniform pressure welding. On this basis, the effects of welding process parameters and magnet structure parameters on the welding quality and welding area of the joint are further studied, which provides a theoretical and experimental basis for increasing the welding area and improving the welding quality.

Keywords Magnetic pulse welding · Uniform pressure electromagnetic actuator · Optimal design · Welded joints · Welding quality · Welding area

1 Introduction

With the rapid development of transportation industry and the improvement of energy conservation and consumption reduction requirements, the lightweight of transportation vehicles has become an inevitable trend driven by the times [1]. Aluminum alloy has the advantages of light weight, high specific strength, and corrosion resistance. It has become one of the important raw materials for the lightweight of vehicles [2]. At the same time, in the production of transportation equipment, the connection mode of materials has gradually changed from single steel connection to diversified connections such as steel-aluminum and aluminum-aluminum. However, due to the significant differences in

physical and chemical properties of dissimilar metals, it is difficult to achieve high-quality welding by traditional fusion welding [3]. As a novel high-speed impact welding technology, magnetic pulse welding uses pulsed electromagnetic force to drive the workpiece to be welded to collide at high speed, which can realize the metallurgical combination of different metals and it has the advantages of high welding strength, no pollution, and easy automation [4–7].

According to the different structures of weldments, magnetic pulse welding is mainly divided into two categories: pipe fitting and plate welding [8, 9]. At present, the research on magnetic pulse welding technology of pipe fittings is relatively mature and has a wide range of industrial applications [10, 11]. Relatively speaking, the magnetic pulse welding technology of plates is not mature enough and is still in the initial exploration stage. It mostly adopts the form of single turn conductor, which has the problems of low utilization rate of welding energy and easy deformation and damage of coils, which is not conducive to repeated experiments and industrial production, and has certain limitations [12, 13].

✉ Hongfa Ding
dhf@hust.edu.cn

1 Wuhan National High Magnetic Field Center, Huazhong University of Science and Technology, Wuhan 430074, China

The magnetic pulse welding method based on uniform pressure electromagnetic actuator adopts multi-turn coil structure, which not only improves the energy utilization rate, but also ensures the mechanical strength of the coil.

Weddeling et al. and Yu and Tong verified the feasibility of using uniform pressure coil to realize magnetic pulse welding of the same and different metal plates from the experimental aspect, but did not optimize the structural parameters of the uniform pressure welding device [14, 15]. In addition, by studying the influence law of different welding process parameters and magnet structure parameters on the welding quality and welding area of the joint, it is helpful to adjust and control the welding parameters, increase the welding area, obtain high-quality welded joints, and further guide the optimal design of welding equipment. Therefore, it is necessary to conduct further research.

In this paper, the COMSOL finite element software is used to analyze the influence of various structural parameters of the magnet device on the distribution characteristics of the magnetic pressure on the surface of the workpiece, and the welding device with different structural parameters is optimized and designed. Then, the uniform pressure welding experimental platform was built, and a series of surface welding experiments were carried out on AA1060 aluminum plate and SS304 stainless steel plate. The mechanical properties of the welded joints were tested through tensile and stripping experiments, and the corresponding welding process parameters were determined. Finally, the effects of welding process parameters and structural parameters on welding quality and welding area are studied through experiments, which provides a theoretical and experimental basis for increasing welding area and improving welding quality.

2 Basic principle and numerical model

2.1 Basic principle

The schematic diagram of uniform pressure welding is shown in Fig. 1, which is mainly composed of power supply system, discharge coil, conductive channel, plate, and cushion block. The conductive channel is fixed on the aluminum plate by applying external pressure to form a closed circuit. The coil is embedded in the conductive channel, and the gap between the aluminum plate and the stainless steel plate can be adjusted through the cushion block. During operation, the power supply system first generates current I_s through coil discharge, and then the induced eddy current I_c will be generated in the closed circuit composed of conductive channel and aluminum plate. The current further generates strong magnetic field B_s in the air gap inside the coil, and generates strong magnetic field B_c in the air gap between the closed circuit composed
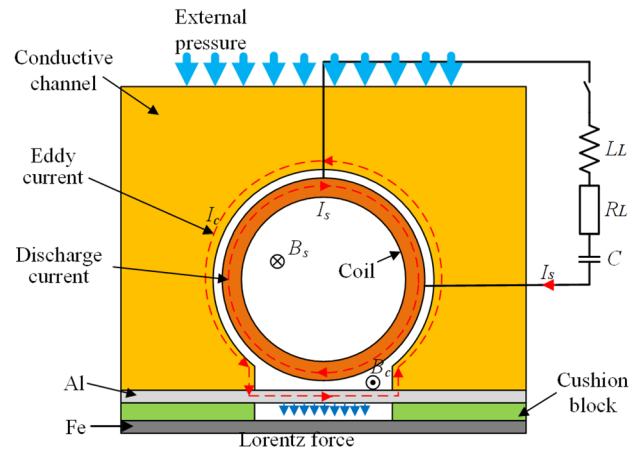

Fig. 1 Schematic diagram of uniform pressure welding

of conductive channel to aluminum plate and the coil. Under the joint action of strong magnetic field B_c and induced eddy current I_c, aluminum plate will be subjected to huge electromagnetic repulsion force to produce plastic deformation movement, and finally collide with stainless steel plate at high speed to realize welding.

2.2 Establishment of numerical model

In order to analyze the influence of structural parameters on the magnetic pressure on the workpiece surface, a three-dimensional model of uniform pressure welding system is established by using the COMSOL finite element software. As shown in the simulation flowchart in Fig. 2, the whole welding system is composed of five physical modules. In order to save the calculation cost and improve the optimization design efficiency, only the circuit and magnetic field modules are used in the optimization, and finally five modules are used in the magnet verification.

2.2.1 Global ODE and DAE module

This module is used for the circuit analysis of the welding system. The uniform pressure welding system can be equivalent to the equivalent circuit shown in Fig. 3. According to the equivalent circuit, the following differential equations can be listed, and the discharge current in the coil can be obtained by solving the equations.

$$I_s R_L + L_L \frac{dI_s}{dt} + V_{coil} = U_c \tag{1}$$

$$U_c = -\frac{1}{C} \int_0^t I_s dt \tag{2}$$

Fig. 2 Simulation flowchart by using COMSOL
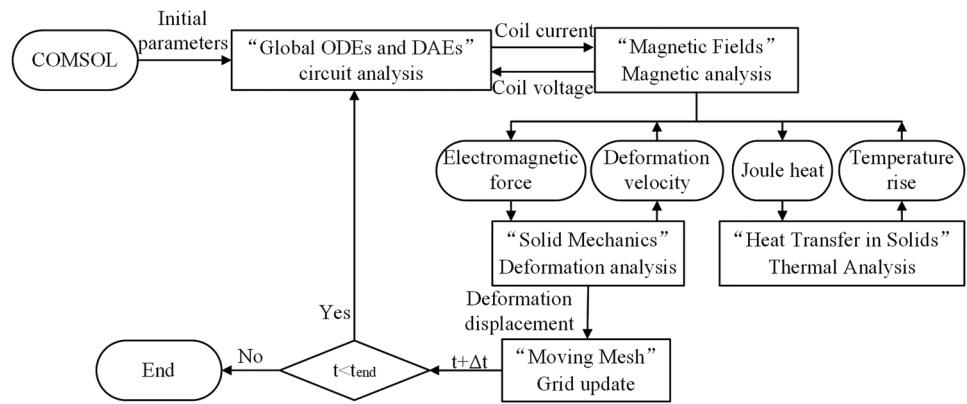
$$V_{coil} = R_{eq}I_s + L_{eq}\frac{dI_s}{dt} \tag{3}$$

Equation (1) is the voltage balance equation of the discharge circuit, including capacitor voltage U_c, line voltage $I_sR_L + L_L dI_s/dt$, and coil voltage V_{coil}, where R_{eq} and L_{eq} are the equivalent resistance and inductance of the coil-plate-channel system respectively. The model realizes the coupling between the coil, plate, and channel through these two parameters. The circuit parameters during simulation are listed in Table 1.

2.2.2 Magnetic field module

The module is used for magnetic field analysis of welding device. Firstly, the spatial distribution of magnetic field is solved by Maxwell equation, and then the electromagnetic force acting on the workpiece is calculated and transmitted to the solid mechanics module as the input load. In addition, the Joule heat obtained in the electromagnetic calculation will be transmitted to the solid heat transfer module as a heat source. The electromagnetic parameters during simulation are listed in Table 2.

In this module, the induced eddy current in the coil, channel, and workpiece can be described by the following equation:

$$\nabla \times E = -\frac{\partial B}{\partial t} + \nabla \times (v \times B) \tag{4}$$

$$J = \gamma E \tag{5}$$

where E is the electric field intensity, B is the magnetic flux density, v is the deformation speed of the workpiece, J is the induced current density, and γ is the conductivity of metal materials.

The electromagnetic force F received by the coil and workpiece is determined by the induced eddy current and magnetic flux density, as shown in the following formula.

$$F = J \times B \tag{6}$$

2.2.3 Solid mechanics module

The module is mainly used for the stress analysis of the discharge coil and the plastic deformation movement of the workpiece. Its output will be fed back to the magnetic field

Fig. 3 Equivalent circuit of uniform pressure welding system
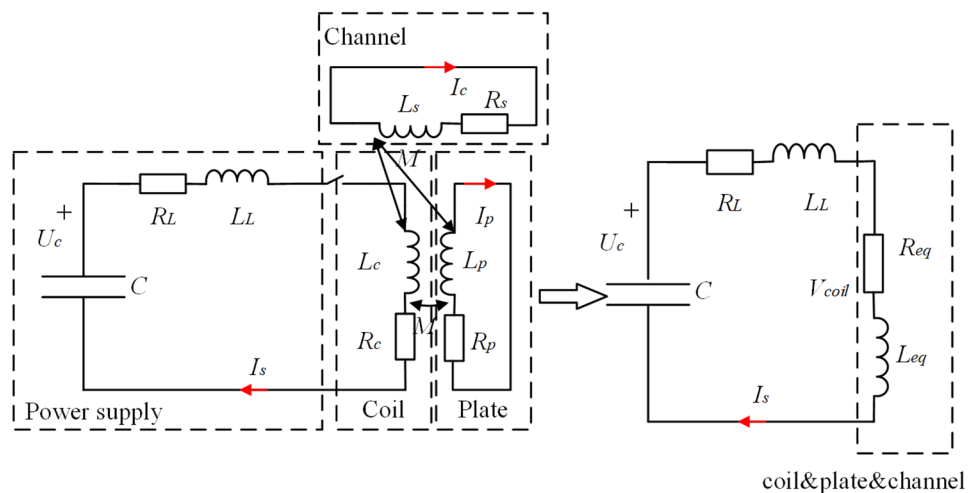
Table 1 Circuit parameters

Symbol	Description	Value
C	Capacitance	150 μF
R_L	Line resistance	22 mΩ
L_L	Line inductance	2.1 μH
U	Discharge voltage	9/10/11 kV

module, so as to realize the coupling calculation of the magnetic field and the structure. The detailed mechanical parameters of materials used in the simulation are given in Table 3.

The workpiece will undergo plastic deformation movement under the action of electromagnetic force, and its motion satisfies the following equation:

$$\nabla \cdot \sigma + \boldsymbol{F}_v = \rho \frac{\partial^2 \boldsymbol{u}}{\partial t^2} \tag{7}$$

where σ is the stress tensor of the workpiece, $\boldsymbol{F}_v$ is the bulk density vector of the electromagnetic force, ρ is the workpiece density, and $\boldsymbol{u}$ is the displacement vector.

The Cowper-Symonds constitutive model is used to consider the effect of high strain rate on the high-speed deformation motion of the aluminum plate during welding. The constitutive equation is expressed as follows:

$$\sigma = \sigma_{qs}\left[1 + \left(\frac{\varepsilon_P^*}{P}\right)^m\right] \tag{8}$$

where σ_{qs} represents the stress–strain equation of AA1060 aluminum plate under quasi-static state, ε_P^* which is the strain rate, and P and m are constants reflecting the effect of high strain rate, with values of 6500 and 0.25 respectively [16].

In order to obtain the stress–strain equation of AA1060 aluminum plate under quasi-static state, the tensile mechanical properties of AA1060 aluminum plate under quasi-static state are tested by universal tensile testing machine. After deep drawing, the load and small displacement curve are obtained, and the real stress–strain curve of the material is obtained after data processing, as shown in

Table 2 Electromagnetic parameters

Material types	Resistivity (γ)	Permeability (μ)
Workpiece		
AA1060	3.53×10^7 S/m	$4\pi \times 10^{-7}$ H/m
SS304	1.35×10^6 S/m	$4\pi \times 10^{-7}$ H/m
Coil		
Copper	5.71×10^7 S/m	$4\pi \times 10^{-7}$ H/m
Channel		
CuCrZr	4.52×10^7 S/m	$4\pi \times 10^{-7}$ H/m

Table 3 Detailed mechanical parameters of materials

| Material types	Density	Yield stress	Young modules	Poisson ratio
Workpiece				
AA1060	2.7×10^3 kg/m³	35 MPa	80.7 GPa	0.34
SS304	7.93×10^3 kg/m³	280 MPa	220 GPa	0.25
Coil				
Copper	8.9×10^3 kg/m³	135 MPa	110 GPa	0.34
Channel				
CuCrZr	8.93×10^3 kg/m³	495 MPa	117 GPa	0.34

Fig. 4. There is no high-speed plastic deformation in the structural analysis of stainless steel plate, so only bilinear isotropic hardening model is needed.

2.2.4 Hot transfer in solid module

This module is mainly used to calculate the temperature rise of the coil. The rise of the coil temperature will not only affect the resistance of the coil, thus affecting the discharge current, but also affect the service life and working efficiency of the coil. Moreover, when the temperature is too high, it will also affect the insulation of the coil, resulting in accidents. Therefore, it is necessary to calibrate the temperature rise to ensure the safety of the experiment.

2.2.5 Moving mesh module

The module is mainly used to update the air grid near the workpiece during the deformation process, so as to avoid the problems of large solution error and non-convergence caused by the distortion of air grid.
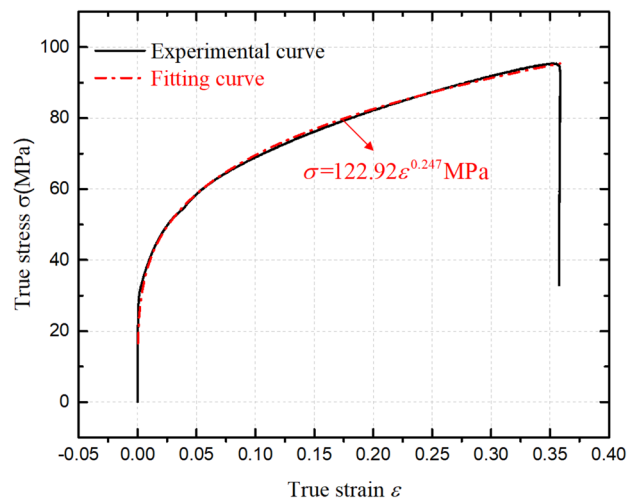
Fig. 4 Experimental and fitting curve of stress and strain of AA1060 aluminum plate under quasi-static state
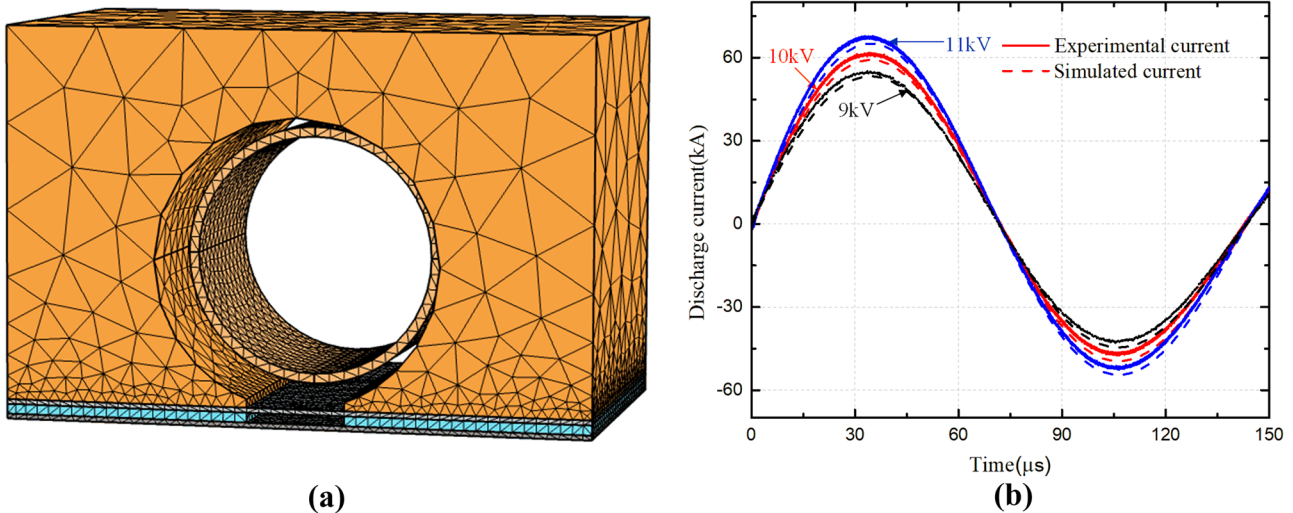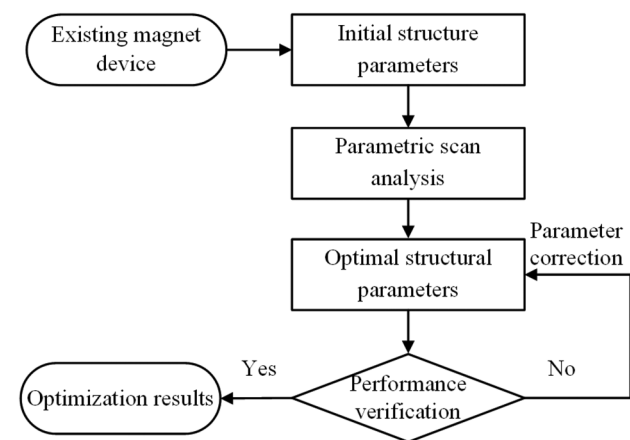
Fig. 5 Finite element model. **a** Geometric entity model. **b** Comparison between simulation waveform and experimental waveform of discharge current

The geometric entity model and grid division of the welding device established by COMSOL are shown in Fig. 5a. In order to verify the reliability and calculation accuracy of the model, the waveforms of the current calculated by the finite element model and the current measured by the experiment under different discharge voltages are given in Fig. 5b. It can be seen that the two waveforms are basically consistent in the first half cycle, which can fully meet the needs of the early optimization design of the welding device.

3 Optimal design of magnet device

Based on the existing magnetic pulse welding power supply device in the laboratory, this paper optimizes the structural parameters of the uniform pressure welding magnet device.
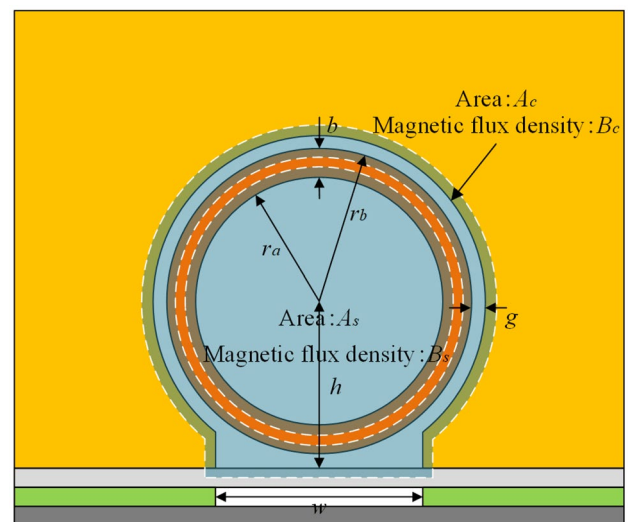
Firstly, a set of initial structural parameters are determined according to the existing uniform pressure welding device. Then, the parametric scanning function of the finite element model is used to analyze the influence of each structural parameter on the magnetic pressure on the surface of the plate. Finally, the optimal structural parameters of the device are obtained. The optimization process is shown in Fig. 6.

3.1 Optimization parameters and objectives

As shown in Fig. 7, it is the geometric model of the uniform pressure welding magnet device, in which B_c and B_s represent the magnetic flux density inside and outside the coil, and A_c represents the equivalent cross-sectional area


Fig. 6 Flowchart of optimization design

Fig. 7 Geometric model of magnet device

Table 4 Initial structural parameters of magnet device

Parameters	Description	Value
N	Turns of coil	10
r_b	Outer radius of coil	27 mm
g	Gap	2 mm
w	Opening width of channel	40 mm
h	Height of coil center	29 mm

of B_c and B_s evenly distributed in their respective magnetic circuits along the length direction of the coil.

The discharge coil adopts a cylindrical coil and is tightly wound with a square copper enameled wire with a cross section of 4 mm×2 mm commonly used in the laboratory. The inter-turn distance is about 0.5 mm. The gap between the coil and the conductive channel is mainly the thickness of the coil wire insulation layer and reinforcement layer. Due to the skin effect, the induced current is mainly distributed on the inner wall of the conductive channel, and the external structure size of the conductive channel is only to ensure its mechanical strength, and has little effect on the eddy current distribution and magnetic pressure, which is set to $120 \times 74 \times 80$ mm^3 here. In addition to the above basic process parameters, the parameters that need to be further optimized for the coil and the conductive channel are mainly the number of turns N of the coil, the outer radius r_b of the coil, the height h of the center of the coil, the width of the opening of the conductive channel w, and the gap g between the coil and the conductive channel, and the initial structural parameters are shown in Table 4.

The research shows that the magnetic pressure on the surface of the workpiece can better reflect the stress distribution of the workpiece. Therefore, the maximization of the magnetic pressure can be taken as the optimization goal, and the optimization design of the magnet device can be described as a single objective optimization problem in a non-strict sense. The optimization equation is:
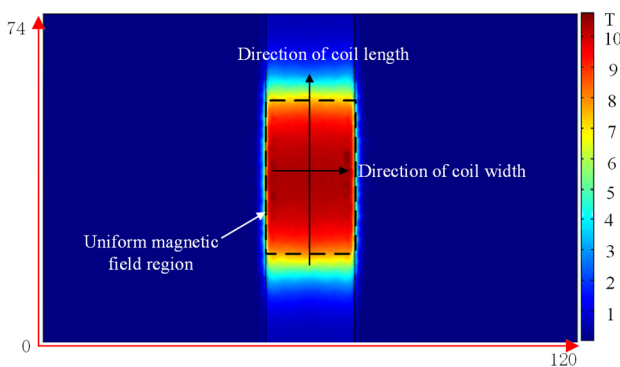
$$\max P = \frac{B^2}{2\mu_0} = \frac{A_s^2 \mu_0 I_s^2}{2(A_c + A_s)^2 k^2} = f(N, r_b, h, w, g) \tag{9}$$

$$T < T_m, \ \sigma < \sigma_s \tag{10}$$

where Eq. (9) is the function expression of single objective optimization, that is, the relationship between the magnetic pressure and the structural parameters of each magnet, and k is the constant related to the coil filling coefficient; Eq. (10) is the constraint condition of single objective optimization, that is, the stress and temperature limit of the magnet itself.

3.2 Analysis of the influence of structural parameters on magnetic pressure

In order to optimize the design of uniform pressure welding magnet device, firstly, the influence of some structural parameters on the magnetic pressure on the surface of workpiece is analyzed according to the analytical equation of magnetic pressure on the surface of workpiece. Then, combined with the parametric scanning function of the finite element model previously established by COMSOL, other structural parameters that need to be optimized are scanned and solved, the influence of each parameter on the magnetic pressure on the surface of plate is explored, and the results are explained and analyzed.

According to Eq. (9), reducing the air gap area A_c and increasing the area can increase the magnetic pressure on the workpiece. Combined with the structural model of the uniform pressure welding device, the analysis shows that reducing the gap g between the coil and the conductive channel and the height h of the coil center can reduce the air gap area A_c and increase the magnetic pressure on the workpiece. The gap g is determined by the thickness of the coil insulation layer and reinforcement layer. If it is too small, the strength of the coil and the insulation strength between the coil and the conductive channel cannot be guaranteed. The smaller the gap g is, the better it is on the premise of ensuring the strength of the coil. In the design, it is necessary to ensure that the coil after insulation reinforcement can exactly match with the conductive channel. When the reinforced coil is exactly tangent to the workpiece surface, the minimum h can be guaranteed. The influence of other structural parameters on magnetic pressure is complex, which needs to be further analyzed and discussed in combination with the finite element model.

As shown in Fig. 8, for the magnetic field distribution results on the workpiece surface obtained by finite element model simulation, it can be seen that the magnetic field distribution in the corresponding area of the coil on the workpiece is relatively uniform, and the magnetic field

Fig. 8 Magnetic field distribution on workpiece surface
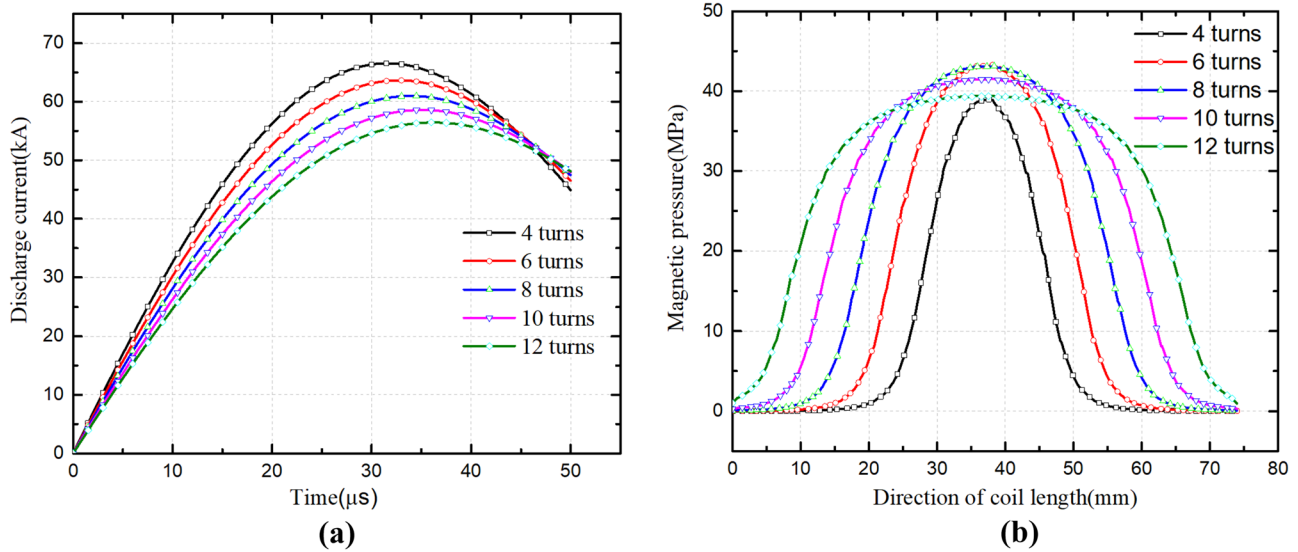
Fig. 9 Simulation results under different coil turns. **a** Discharge current. **b** Magnetic pressure in the direction of coil length

at both ends of the coil length direction is small due to the influence of edge effect. In order to quantitatively analyze the influence of other structural parameters on the specific distribution characteristics of the magnetic pressure on the workpiece surface, the distribution curves of the magnetic pressure on the workpiece along the length and width of the coil in Fig. 7 are further drawn under different structural parameters.

3.2.1 Influence of coil turns

Figure 9 shows the comparison of simulation results of discharge current and magnetic pressure on the workpiece surface under different coil turns while keeping the discharge voltage and other parameters unchanged. It can be seen from the figure that with the increase of coil turns, the discharge current shows a continuous decreasing trend, while the magnetic pressure on the workpiece surface shows a trend of increasing first and then decreasing. This is because the magnetic field intensity is positively correlated with the ampere turns NI. The increase of coil turns N will increase the load in the circuit and reduce the current I of the discharge circuit. Therefore, there will be a maximum value of ampere turns NI and magnetic flux density B. The simulation analysis shows that when the number of coil turns is $6 \sim 8$ turns, the magnetic pressure on the surface of the plate is the largest, and the welding effect is the best. Continuing to increase the number of coil turns will reduce the magnetic pressure on the workpiece surface, but will increase the width of the area with uniform magnetic pressure, so as to increase the length of the plate welding area. Therefore, in order to realize the welding of a larger area, it is necessary

to further increase the discharge voltage to ensure the welding strength.

3.2.2 Influence of outer radius of coil

As shown in Fig. 10, the simulation results of discharge current and magnetic pressure on workpiece surface under different outer radius of coil are compared. It can be seen from the figure that with the increase of r_b, the discharge current continues to decrease, while the magnetic pressure on the workpiece surface first increases and then decreases. According to the analysis of Eq. (9), the increase of r_b will first lead to the increase of coil impedance, so the discharge current will show a decreasing trend, and the decrease of discharge current will lead to the decrease of magnetic pressure. While the increase of r_b will also lead to the increase of A_s, the increase of A_s will lead to the increase of magnetic pressure. In the initial stage, the increase of magnetic pressure caused by the increase of A_s is dominant, so the magnetic pressure increases first. When r_b reaches a certain value, the size of A_s is much larger than A_c; at this time, $A_s/(A_s + A_c)$ basically does not change, while the increase of r_b will still lead to the decrease of discharge current, so it will lead to the decrease of magnetic pressure.

3.2.3 Influence of opening width of conductive channel

Figure 11 is a comparison of the simulation results of the magnetic pressure on the workpiece surface in the length direction and width direction of the coil with the discharge voltage and other parameters unchanged. It can be seen from
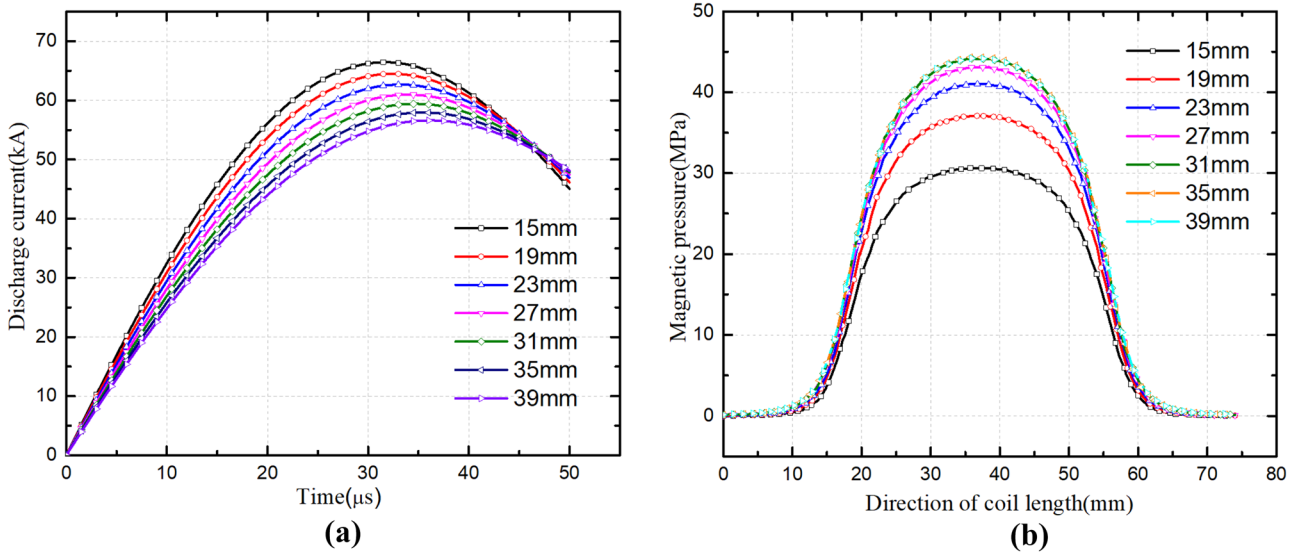
Fig. 10 Simulation results under different coil outer radius. **a** Discharge current. **b** Magnetic pressure in the direction of coil length

the figure that with the increase of the opening width w of the conductive channel, the magnetic pressure in the length direction and width direction of the coil shows a continuous decreasing trend, because the increase of w will increase the air gap area A_c, resulting in the decrease of the magnetic pressure. In addition, with the increase of w, the uniform area in the width direction of the coil will become wider. To sum up, the increase of w will increase the uniform area of magnetic pressure in the width direction of the coil, that is, it will increase the width of the welding area, but it will also reduce the amplitude of magnetic pressure on the surface of the workpiece. Therefore, it is necessary to select the opening width of the conductive channel according to the actual demand.

3.3 Optimization results

It can be seen from the above analysis that the smaller the gap g between the coil and the conductive channel, the greater the magnetic pressure. Considering the coil insulation and reinforcement, it is designed as 2 mm here. The opening width w of the conductive channel determines the width of the welding area, but the magnetic pressure on the workpiece surface will decrease with the increase of the opening width w of the conductive channel, which should be selected according to the welding requirements. There is an optimal value for the outer radius of the coil. The simulation analysis shows that when the outer radius of the coil
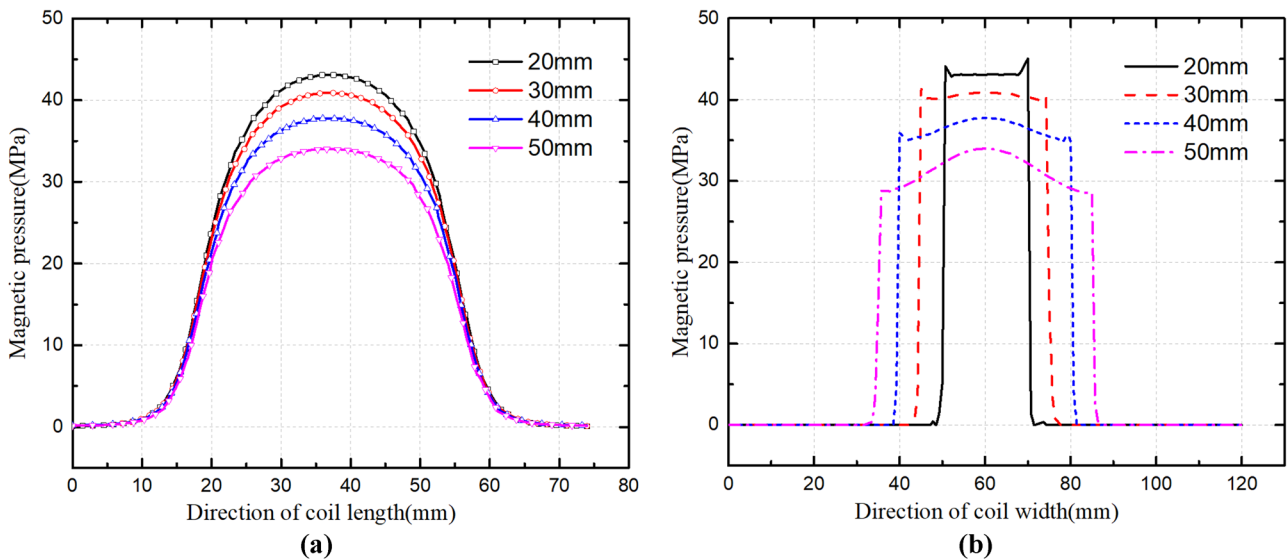

Fig. 11 Simulation results of magnetic pressure under different opening widths. **a** Direction of coil length. **b** Direction of coil width

Table 5 Optimized structural parameters

Parameters	Description	Value
N	Turns of coil	8/10/12
r_a	Inner radius of coil	27 mm
r_b	Outer radius of coil	30 mm
g	Gap	2 mm
w	Opening width of channel	20/30/40 mm
r_c	Inner radius of channel	32 mm
h	Height of coil center	32 mm

is about 30 mm, the magnetic pressure on the workpiece surface is the largest. There is an optimal value for the number of coil turns. The simulation results show that when the number of coil turns is 6 ~ 8 turns, the magnetic pressure on the workpiece surface is large, and the welding effect is the best at this time, but the number of coil turns determines the length of the welding area, which also needs to be selected according to the actual welding requirements.

Based on the partial optimization of the magnet device, a uniform pressure welding magnet device with different coil turns and conductive channel opening width is designed to further verify the above analysis through experiments. The main parameters after optimization are shown in Table 5, and the electromagnetic, mechanical, and thermal properties of the optimized magnetic device are verified, which can meet the experimental requirements.

4 Experiment

### 4.1 Construction of experimental platform

In order to realize the uniform pressure surface welding experiment of aluminum/steel metal plates, a high-performance uniform pressure magnet device was developed in this section, and a complete uniform pressure welding platform was designed and built, including a pulse power supply device and a magnet device. The pulse power supply device adopts the existing capacitive power supply in the laboratory including a power supply of 200 kJ, a high pressure pneumatic switch, and a capacitor bank of 150 μF with a peak voltage of 20 kV, as shown in Fig. 12.

The welding coil used by the device is a single-layer multi-turn cylindrical coil. Because the coil is mainly affected by inward electromagnetic force, in order to ensure the strength of the coil, the epoxy rod is used as the skeleton, and then the flat copper conductor with a section of 2 mm × 4 mm is tightly wound on the coil skeleton. In order to ensure the insulation strength of the coil conductor, a layer of high-voltage insulating tape is wrapped outside the original insulating layer of the copper conductor. After the coil is wound, a layer of Zylon fiber is first wound on the outer layer of the coil, which can fill the gap between turns and reinforce it. Then, a layer of glass fiber is wound on the outermost layer and impregnated with liquid epoxy adhesive. After the epoxy adhesive is cured, the reinforced coil is turned so that the coil can be highly matched with the conductive channel, as shown in Fig. 13a. In order to ensure that the air gap is as small as possible, the insulation reinforcement layer is designed as 2 mm to ensure the insulation strength between the coil and the conductive channel. The conductive channel is made of Cu-Cr-Zr with high melting point and high hardness, and its inner radius just matches the reinforced coil. In order to study the influence of the opening width of the conductive channel on the welding area, the conductive channel with different opening widths is designed and processed, as shown in Fig. 13b.

In order to ensure good electrical contact between the workpiece and the conductive channel, firstly, the contact surface between the conductive channel and the workpiece is polished and cleaned with alcohol to remove burrs and stains on the surface. Then, apply a layer of uniform conductive paste on the contact surface between the conductive channel and the workpiece to reduce the contact resistance between the workpiece and the conductive channel, so as to reduce or even eliminate the ignition and ablation phenomenon

Fig. 12 Power system. **a** Power supply. **b** High pressure pneumatic switch. **c** Capacitor bank

(a)	**(b)**	**(c)**
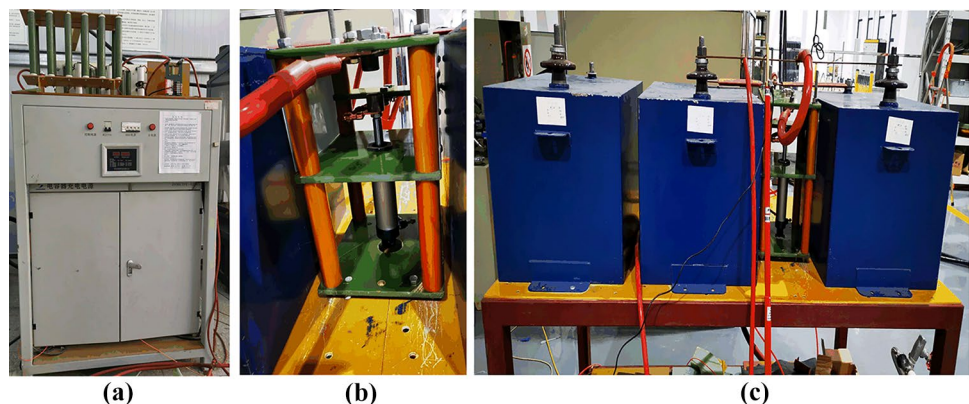
Fig. 13 Welding device components. **a** Coils with different turns. **b** Conductive channels with different opening widths

(a)   (b)
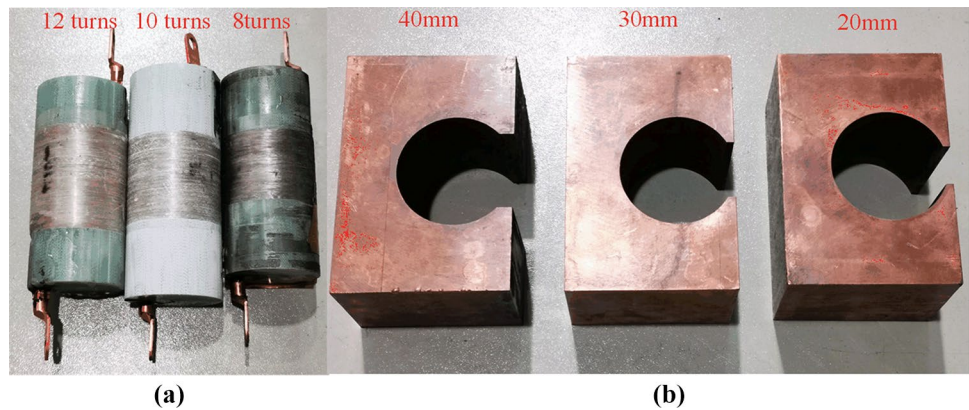
in the discharge process, as shown in Fig. 14a. Finally, the conductive channel, coil, and workpiece are reinforced with two stainless steel end plates and bolts to provide sufficient pressure to prevent the separation of the conductive channel and the workpiece caused by the huge repulsive force during the discharge process, resulting in an air gap, which leads to breakdown discharge, as shown in Fig. 14b. The workpiece is placed on the surface of the conductive channel where the conductive paste is applied, and the workpiece is separated from the stainless steel plate by a spacer. The acceleration gap of the workpiece can be adjusted by selecting spacers with different thicknesses.

4.2 Experimental scheme

Discharge voltage and welding gap are the key process parameters that determine the success or failure of welding and affect the welding quality. Among them, the discharge voltage determines the output energy of the system, and finally determines the collision speed; the welding gap determines the acceleration distance of the workpiece, which will affect the collision speed and collision angle. In addition, the opening width of the conductive channel and the number of turns of the coil directly affect the size of the welding area and the deformation behavior of the

workpiece in the welding process. In order to study the influence of the above process parameters and structural parameters on the welding results, the following experiments are designed:

1. The designed welding device is used to carry out welding experiments on the workpiece under different welding gaps and different discharge voltages to study the influence of discharge voltage and welding gap on the welding results. The discharge voltage is from 8 to 11 kV, and the welding gap is 2 mm, 2.5 mm, 3 mm, 3.5 mm, and 4 mm respectively.
2. The welding gap and the opening width of the conductive channel were fixed, and the welding experiments were carried out on the workpiece with different turns of coils under different discharge voltages to study the influence of the number of coil turns on the morphology and welding area of the welding area.
3. The welding gap and the number of coil turns are fixed, and the welding experiments are carried out on the workpiece by using conductive channels with different opening widths under different discharge voltages to study the influence of the opening width of the conductive channels on the morphology and welding area of the welding area.

Fig. 14 Welding device. **a** Apply conductive paste on the contact surface. **b** Welding device reinforcement

(a)   (b)
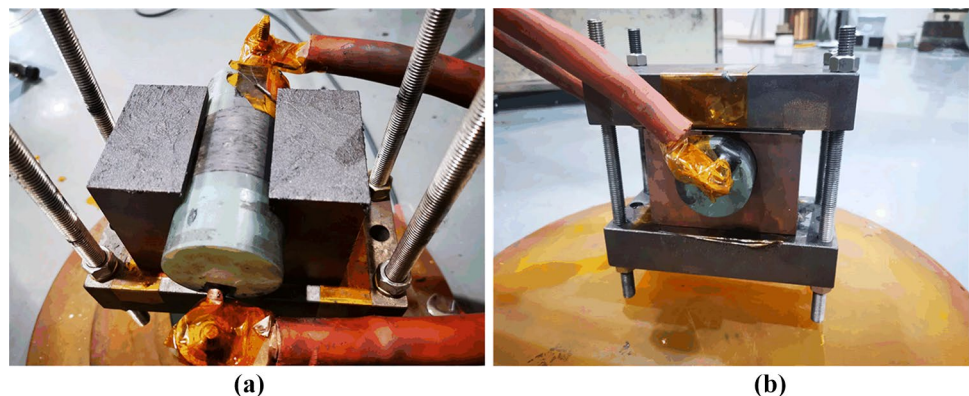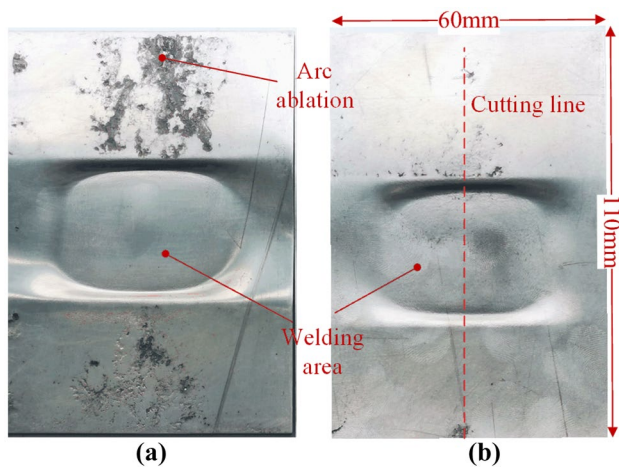
Fig. 15 Welding sample. **a** Uncoated with conductive paste. **b** Coated with conductive paste

4.3 Welding results and mechanical property analysis

4.3.1 Appearance and section analysis of welding area

In this section, the appearance and cross section of the welded area were analyzed for the welded samples with a discharge voltage of 11 kV and a welding gap of 3 mm. Figure 15 shows the appearance of the welding sample obtained when the contact surface is not coated with conductive paste and coated with conductive paste. It can be seen from the figure that the deformation in the middle area of the plate is relatively uniform, and the welding area is approximately a rectangular surface, realizing the surface welding of the plates. The surface of the welding sample without conductive paste on the contact surface has a large area of serious ablation area, and the molten workpiece will also adhere to the contact surface of the conductive channel, making the contact surface rough and uneven, making it difficult to repeat the welding experiment, and the ablation area also seriously affects the strength and beauty of the welding sample. After the contact surface is coated with conductive paste, the ablation phenomenon on the surface of the workpiece is greatly reduced because the contact resistance between the conductive channel and the contact surface of the plate is reduced.

In order to further analyze the detailed characteristics of the welded sample, the welded sample was cut along the cutting line in Fig. 15, the cross section of the sample was

analyzed, and the cross-sectional view is shown in Fig. 16. It can be seen from the figure that both area 1 and area 3 are welded, while the central area 2 is not welded and has a certain bulge phenomenon. There are two main reasons for this phenomenon: First, due to the uniform speed of the central area and the small collision angle, although the collision speed is large, it is difficult to form jet to realize metallurgical combination, and rebound after collision to form bulge; second, the air in the central area is not eliminated, resulting in the generation of bulges.

In addition, the thinning and tearing of the workpiece at the chamfer is also a problem in uniform pressure welding. In order to improve this problem, right angle cushion block and oblique angle cushion block are used on both sides of the experiment. The results show that the workpiece at the chamfer appears thinning or even tearing at the end of the right angle cushion block. At the end of the inclined cushion block, because the inclined plane provides a buffer zone for the deformation and collision of the plate, the plate at the chamfer is only slightly thinned, and the experimental verification shows that the inclined angle of the cushion block is about $30 \sim 45°$.

4.3.2 Analysis of mechanical properties of welding samples

In order to examine the bonding strength of the welding interface, a peeling experiment was first performed on the welded sample welded with a 10-turn coil and a conductive channel with an opening width of 40 mm, and the results are shown in Fig. 17. It can be seen from the figure that when the welding strength is low, the workpiece can be stripped, and there are white welding traces on the surface of the stainless steel plate. The welding trace is a square ring, and the center is the unwelded area. At this time, the welding strength is lower than the base metal of the workpiece. When the welding strength is high, the workpiece is torn and the workpiece in the welding area cannot be stripped. At this time, the welding strength is higher than that of the base metal.

In order to further test the bonding strength of the welded joint, the tensile test was carried out on the welded joint samples obtained by welding with the same coil, the same conductive channel, and different discharge voltages (the samples are long strips cut from the welded samples containing the complete welding area), and the tensile displacement curves of the welded joint under different discharge voltages

Fig. 16 Cross section of welding sample
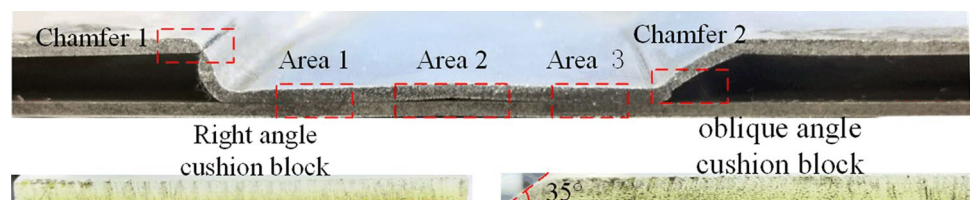
Fig. 17 Peeling test of welding sample. **a** Low welding strength. **b** High welding strength

(a)   (b)

were obtained, as shown in Fig. 18. It can be seen from the figure that when the discharge voltage is 8 kV, the welding sample pulls off at the joint, the welding strength of the joint is lower than that of the base metal, and the welding effect is poor; when the discharge voltage is 9 kV, 10 kV, and 11 kV, the samples are broken at the base metal, indicating that the welding strength of the joint is greater than that of the base metal. In addition, with the increase of discharge voltage, the tensile strength of the sample joint increases first and then decreases, and the maximum tensile strength is slightly smaller than the workpiece base metal, which may be caused by the thinning of the workpiece at the chamfer.

In order to explore the reason, the tensile results of welded samples under different opening widths of conductive channels were compared when the discharge voltage was 10 kV and the welding gap was 3 mm, as shown in Fig. 19. It can be seen from the figure that the base metal fracture occurred in the welding samples, and the fracture location is located at the chamfer, indicating that the thinning of the
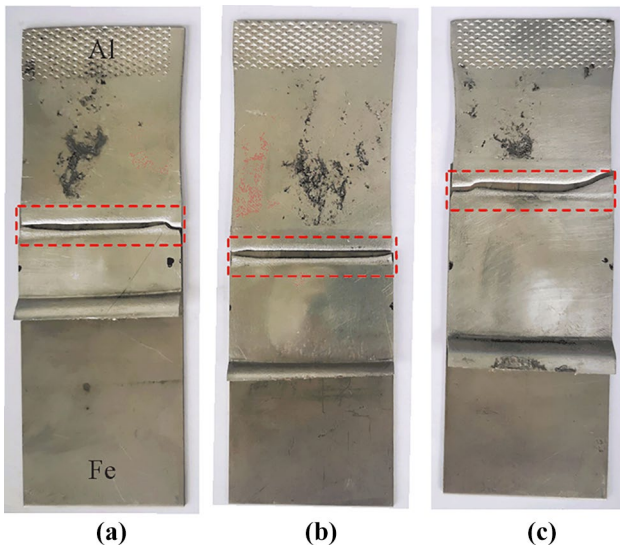
workpiece at the chamfer makes it most prone to fracture failure, and the tensile strength is lower than the base metal of the workpiece. The reason why the tensile strength of welded joints decreases with the increase of discharge voltage is that when the discharge voltage is high, the collision speed is large, the plastic deformation of workpiece is severe, the thinning of chamfered workpiece is also serious, and the tensile strength of joints decreases.

In order to explore the influence of welding gap on joint welding quality, tensile tests were carried out on the welding samples with welding gap of 2 mm, 2.5 mm, 3 mm, 3.5 mm, and 4 mm when the discharge voltage was 10 kV. The tensile strength and failure mode of the welded sample joint are shown in Table 6. It can be seen that when the welding gap is less than 3 mm, the tensile strength of the joint increases gradually. When the welding gap is within 3~4 mm, the tensile strength of the joint decreases gradually, and the failure mode is base metal fracture.

Figure 20 shows the tensile strength curve of the joint under different welding gaps, which increases first and then

(a)   (b)
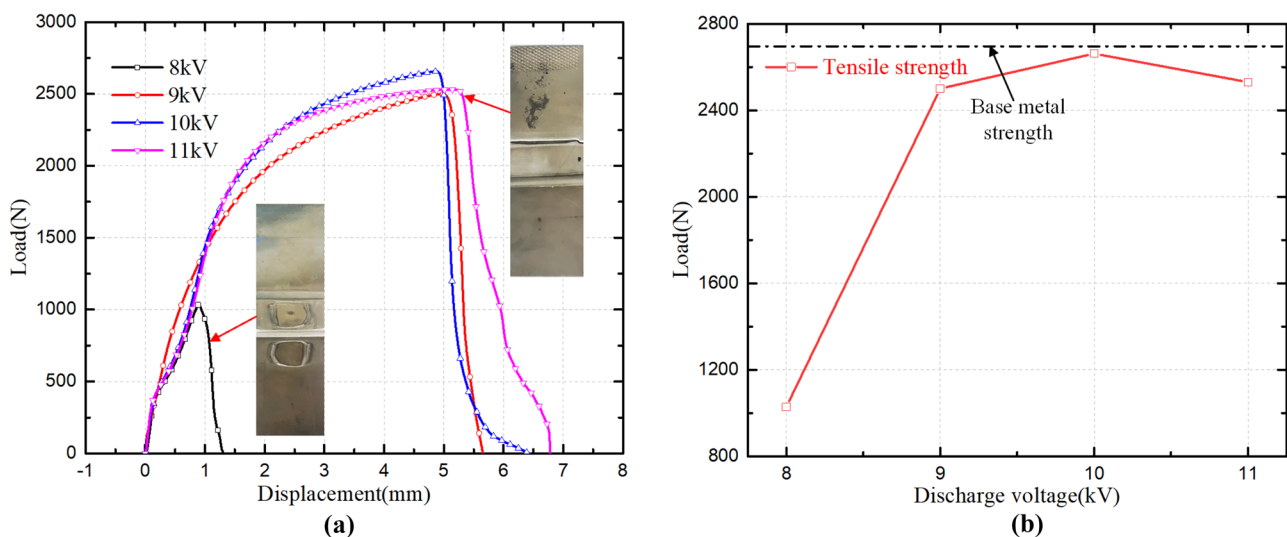
Fig. 18 Tensile test of joint under different discharge voltages. **a** Load–displacement curve. **b** Tensile strength

Fig. 20 Tensile strength of samples under different welding gaps

Fig. 19 Tensile results of samples with different opening widths. **a** 20 mm. **b** 30 mm. **c** 40 mm
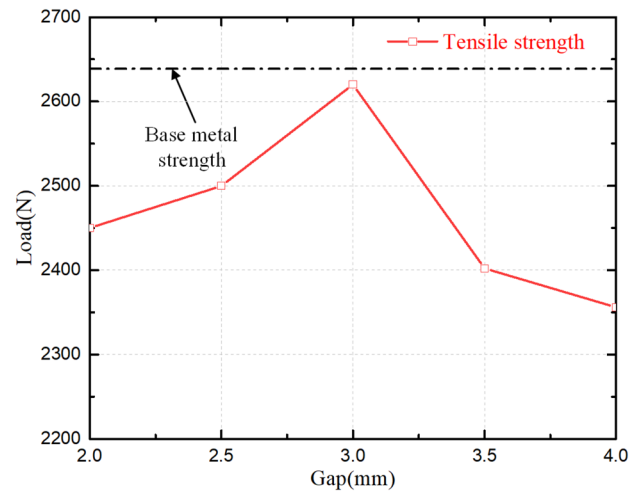
decreases, indicating that there is an appropriate range of welding gaps. When the welding gap is large, the tensile strength decreases significantly, which is mainly due to the serious thinning of the joint chamfer when the welding gap is large. To sum up, in this welding experiment, when the welding gap is 2.5~3.5 mm, the tensile strength and reliability of the joint are high.

4.4 Welding window

Through the above welding experiment and tensile test of welding samples, the welding window of discharge voltage (energy)—welding gap when the number of coil turns is 8 turns and the opening width of conductive channel is 40 mm—is established (the welding window obtained under other combinations is similar), as shown in Fig. 21. It can be seen from the welding window that under this welding

Table 6 Tensile strength and failure mode of joint under different welding gaps

Gap(mm)	Tensile strength(N)	Failure mode
2	2423	Base metal fracture
	2498	Base metal fracture
2.5	2510	Base metal fracture
	2490	Base metal fracture
3	2662	Base metal fracture
	2586	Base metal fracture
3.5	2392	Base metal fracture
	2412	Base metal fracture
4	2396	Base metal fracture
	2316	Base metal fracture

device, when the welding gap is 2.5~3.5 mm, it is more reasonable, the welding can be realized with lower voltage, and it is easy to produce high-quality welded joints. Although the higher the discharge voltage, the easier it is to realize welding, it will also aggravate the thinning of the workpiece at the chamfer, which is not conducive to improving the tensile strength of the joint. Therefore, it is necessary to select an appropriate discharge voltage. The discharge voltage and welding gap need to be well matched to complete the welding process and realize high-quality welding.

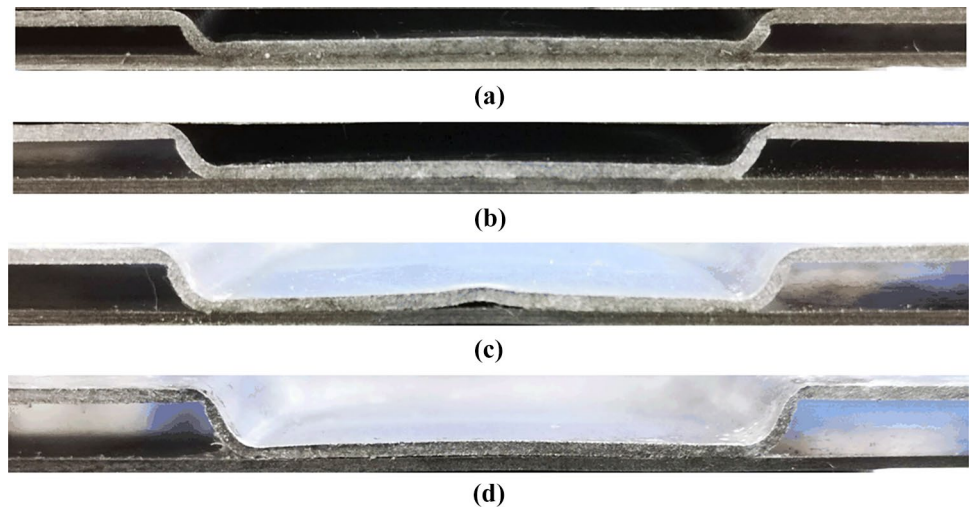### 4.5 Influence of process parameters and structural parameters on welding area

4.5.1 Influence of welding gap

Figure 22 is a cross-sectional view of the welding samples along the coil width obtained under different welding gaps
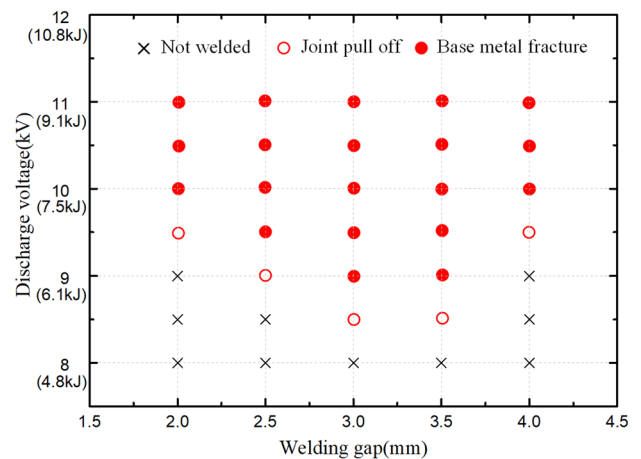
Fig. 21 Discharge voltage (energy)—welding gap welding window

Fig. 22 Sample section under different welding gaps. **a** 2 mm. **b** 2.5 mm. **c** 3 mm. **d** 3.5 mm

(a)

(b)

(c)

(d)

when the discharge voltage is 10 kV. It can be seen from the figure that when the welding gap is 3 mm, the central bulge is more obvious, indicating that the collision speed is higher, the plate collision is more intense, and the rebound in the central area of the plate is also more serious under this welding gap. In addition, with the increase of welding gap, the workpiece thinning at the chamfer will become more and more serious. Therefore, it is necessary to select the appropriate welding gap to achieve high-quality welding.

In order to analyze the effect of welding gap on the morphology of weld bead in the welding area, the morphology of the welding area after corrosion in strong alkali solution was studied. According to the characteristics of strong alkaline solution corroding aluminum and stainless steel, alkaline solution is used to corrode the welded joints of plates. Due to the diffusion of aluminum and iron elements at the position where effective welding is achieved, it will appear dark black after corrosion; however, the position without effective welding will be light gray and stainless steel after corrosion. Figure 23 shows the weld bead morphology of the welding area under different welding gaps. It can be seen from the figure that when the welding gap is between 2 and 3 mm, the welding area tends to become larger with the increase of the welding gap, and the weld bead is also deepened and widened, which is conducive to improving the welding strength of the welded joint. When the welding gap increases to 3.5 mm, the weld bead has become shallower and narrower, which further proves that the welding gap in

an appropriate range is conducive to the realization of high-quality welding.
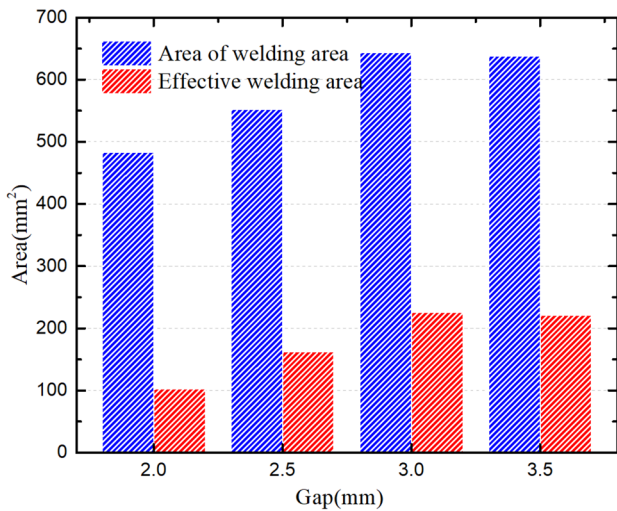
The statistical results of the total welding area and effective welding area under different welding gaps are shown in Fig. 24. It can be seen from the figure that with the increase of the welding gap, the total welding area and the effective welding area show a trend of first increasing and then decreasing, which shows that within a certain range, increasing the welding gap can increase the welding area and the effective welding area. Effective welding area improves the tensile strength of the joint.

4.5.2 Effect of discharge voltage

Figure 25 is a cross-sectional view of the welding sample along the coil width under different discharge voltages. It can be seen from the figure that the central bulge area shows a trend of increasing and widening with the increase of discharge voltage. Through the analysis, it can be seen that because the collision angle of the center is too small to realize the welding, the workpiece rebounds and forms a bulge after the collision. With the increase of discharge voltage, the collision speed of the plate center also increases, and the rebound becomes more serious. Moreover, when the welding of the peripheral area is completed, the air in the central area cannot be discharged, which will also lead to the formation of bulge. In addition, with the increase of discharge voltage, the thinning of workpiece

Fig. 23 Weld bead morphology under different welding gaps. **a** 2 mm. **b** 2.5 mm. **c** 3 mm. **d** 3.5 mm


(a)　　　　　　(b)　　　　　　(c)　　　　　　(d)
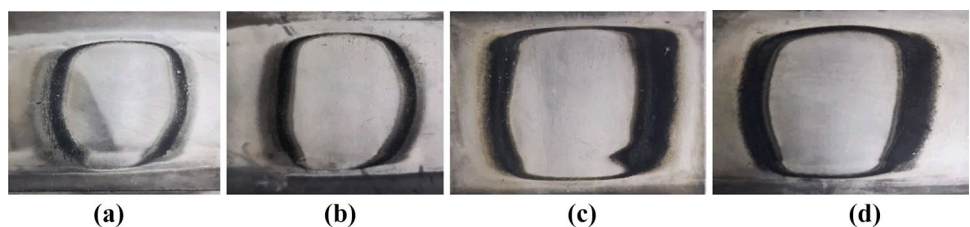
Fig. 24 Total area and effective welding area of welding area under different welding gaps

at chamfer is more serious, which will affect the tensile strength of welded joint.

Figure 26 shows the topography of the weld bead in the welding area under different discharge voltages. It can be seen from the figure that with the increase of the discharge voltage, the weld bead has obvious signs of widening, that is, the effective welding area of the welding area has been significantly increased. This is because the increase of the discharge voltage increases the collision speed of the workpiece, so that the area where the welding cannot be completed with a lower voltage is also welded, thereby increasing the area of the effective welding area, which helps to improve the welding strength of the welded joint. In addition, it can be seen that with the increase of discharge voltage, the upper and lower weld beads tend to move outward, which is also caused by the widening of the bulge area with the increase of discharge voltage.
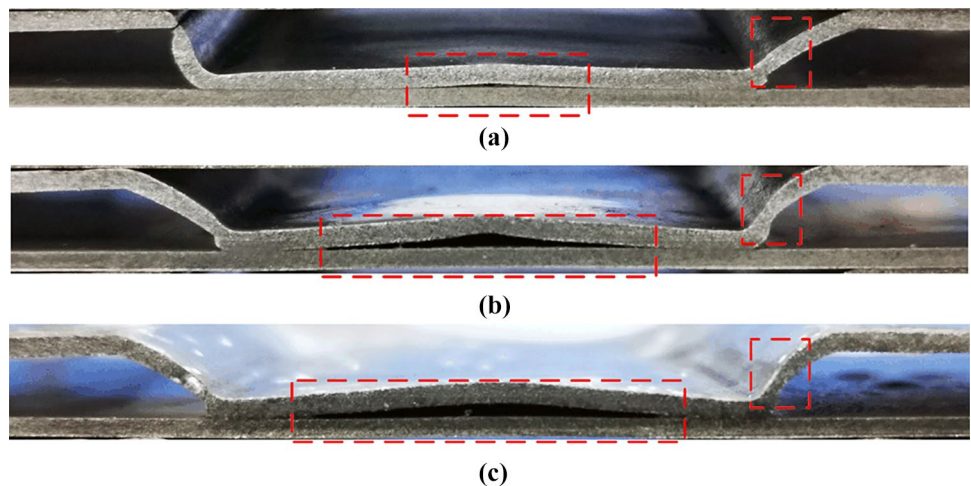
The statistical results of total welding area and effective welding area under different discharge voltages are shown in Fig. 27. It can be seen from the figure that with the increase of discharge voltage, the total area of welding area and effective welding area show an increasing trend, which further shows that increasing discharge voltage can increase the effective welding area and improve the welding strength of the joint.

4.5.3 Influence of opening width of conductive channel

Figure 28 is a cross-sectional view of the welded sample along the coil width direction obtained by using conductive channels with different opening widths when the discharge voltage is 10 kV. It can be seen from the figure that with the increase of the opening width of the conductive channel, the width of the welding area increases, and the central bulge height first increases and then decreases. It can be seen from the analysis that when the opening width of the conductive channel is small, the magnetic pressure is large, the collision speed is also large, the uniform central area is narrow, and the area with zero collision angle is also narrow, which is conducive to the welding of the central area. With the increase of the opening width, the uniform central area becomes wider, but the uniformity does not change much. The area with zero collision angle in the central area becomes wider, which is not conducive to the welding of the central area. With the further increase of the opening width, the collision speed decreases, and the collision rebound of the plate is weakened, which leads to a decreasing trend of the height of the center bulge.

Figure 29 shows the weld bead morphology of the welding area under different opening widths. It can be seen from the figure that the width of the welding area increases significantly with the increase of the opening width of the conductive channel. When the opening width was increased

Fig. 25 Sample cross section under different discharge voltages. **a** 9 kV. **b** 10 kV. **c** 11 kV

(a)

(b)

(c)

Fig. 26 Weld bead morphology under different discharge voltages. **a** 9 kV. **b** 10 kV. **c** 11 kV

(a)   (b)   (c)
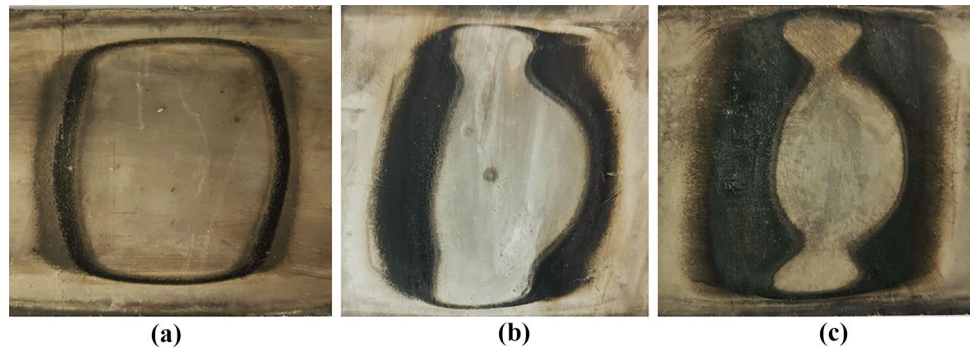
from 20 to 30 mm, the width of the welded area increased from 15 to 24 mm, an increase of 9 mm, and when the opening width was increased from 30 to 40 mm, the width of the welded area increased from 24 to 28 mm, an increase of only 4 mm. This shows that with the increase of the opening width of the conductive channel, the increasing speed of the width of the welding area will slow down, which is mainly due to the decrease of the magnetic pressure on the surface of the workpiece, which leads to the decrease of the collision speed. In addition, with the increase of the opening width of the conductive channel, the weld bead tends to narrow, which is also due to the decrease of the collision speed.

The statistical results of the total welding area and effective welding area under different opening widths are shown in Fig. 30. It can be seen from the figure that with the increase of the opening width of the conductive channel, the total area of the welding area shows an increasing trend, while the effective welding area shows a trend of increasing first and then decreasing, which shows that the increase of the opening width of the conductive channel will increase the total area of the welding area, but when
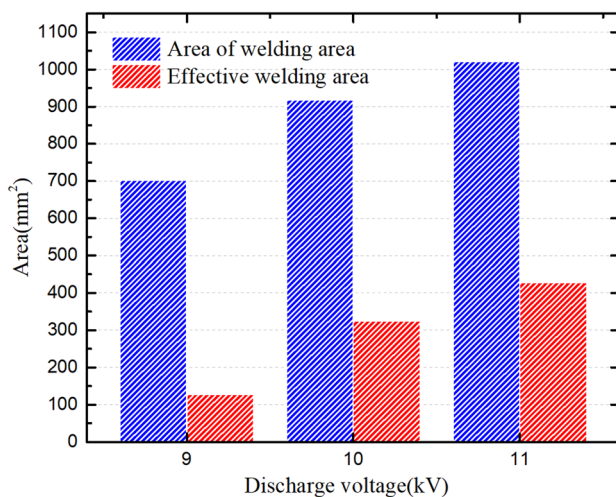
the opening width increases to a certain value, it will lead to a decrease in the effective welding area, resulting in a decrease in the tensile strength of the joint. Therefore, by increasing the opening width of the conductive channel to increase the area of the welding area, the discharge voltage must be increased at the same time to ensure the tensile strength of the joint.

4.5.4 Influence of coil turns

Figure 31 is a cross-sectional view of the welded sample along the length of the coil obtained by using coils with different turns when the discharge voltage is 10 kV. It can be seen from the figure that with the increase of coil turns, the width of the welding area has also increased significantly, while the central bulge area shows a decreasing trend. This is due to the increase of the number of coil turns and the widening of the uniform area of magnetic pressure in the length direction of the coil, so that the workpiece in a larger area can accelerate to the appropriate collision speed and realize welding. Moreover, the increase of the number of coil turns leads to the decrease of the central collision speed and the bulge phenomenon is restrained to a certain extent.

Figure 32 shows the topography of the weld bead in the welding area under different coil turns. It can be seen from the figure that with the increase of the coil turns, the length of the welding area increases significantly, and the width also increases to a certain extent. When the number of coil turns increases from 8 to 10, the length of the welding area increases the most, from 14 to 30 mm, which is more than doubled. When the number of coil turns increases from 10 to 12, the length of the welding area increases from 30 to 40 mm, which is only one-third, indicating that the increase speed of the length of the welding area will also slow down with the increase of the number of coil turns, and this is also due to the decrease of magnetic pressure on the workpiece surface caused by the increase of coil turns, resulting in the decrease of collision speed.
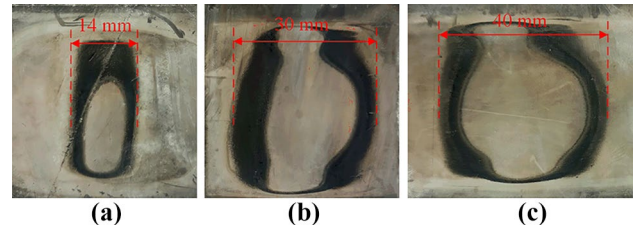
The statistical results of total welding area and effective welding area under different coil turns are shown in Fig. 33.

Fig. 27 Total area and effective welding area of welding area under different discharge voltages
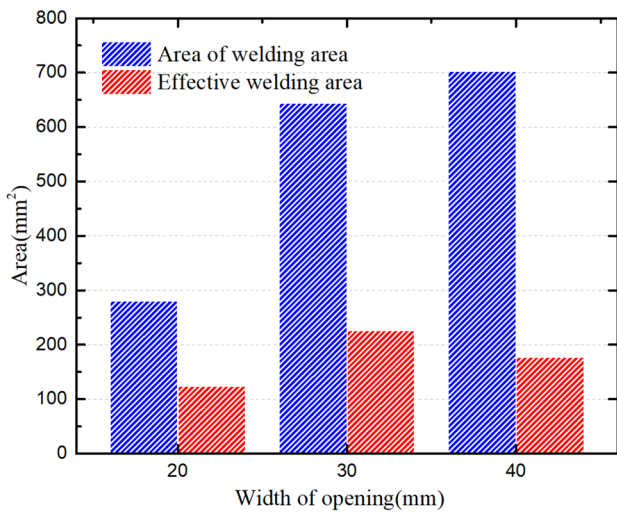
Fig. 28 Sample section under different opening widths. **a** 20 mm. **b** 30 mm. **c** 40 mm
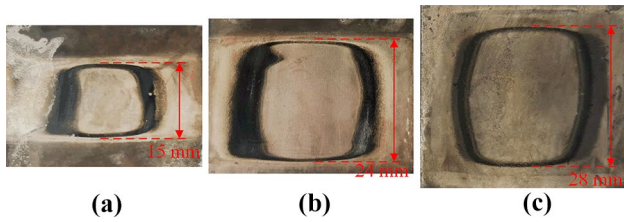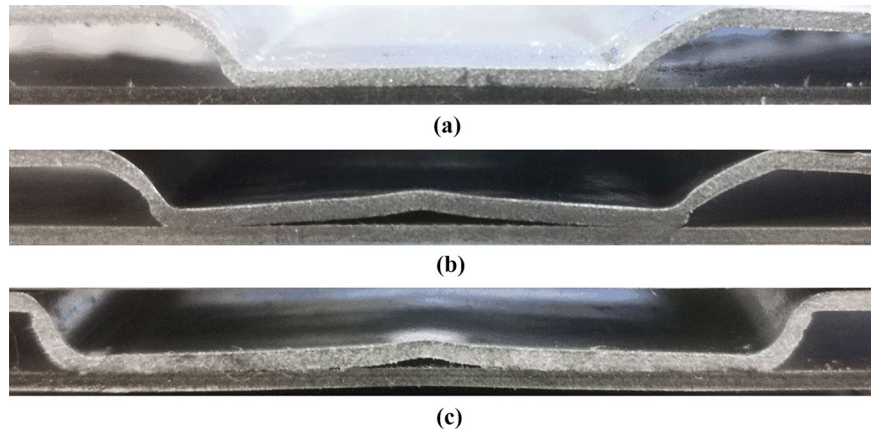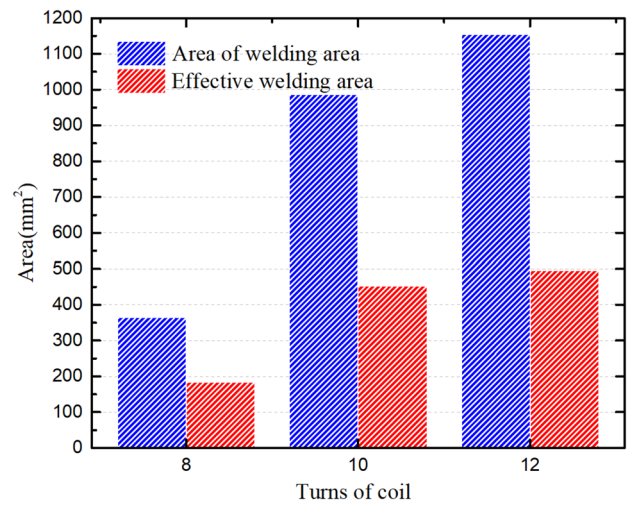

Fig. 29 Weld bead morphology under different opening widths. **a** 20 mm. **b** 30 mm. **c** 40 mm

Fig. 32 Weld bead morphology under different coil turns. **a** 8 turns. **b** 10 turns. **c** 12 turns
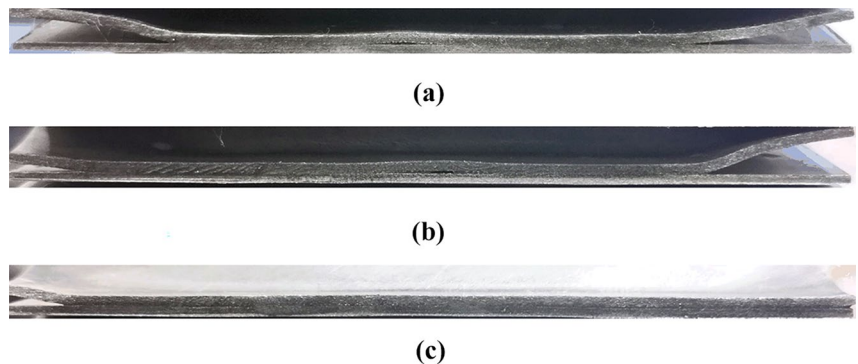

Fig. 30 Total area and effective welding area of welding area under different opening widths

Fig. 33 Total area and effective welding area of welding area under different coil turns

Fig. 31 Sample cross section under different coil turns. **a** 8 turns. **b** 10 turns. **c** 12 turns

It can be seen from the figure that with the increase of the number of coil turns, the total area and effective welding area of the welding area show an increasing trend, but the increasing trend slows down, which shows that within a certain range, increasing the number of coil turns can increase the total area and effective welding area of the welding area. If you want to further increase the number of coil turns to increase the welding area, you also need to increase the discharge voltage to ensure the welding quality of the joint.

5 Conclusion

Aiming at maximizing the magnetic pressure, this paper puts forward the optimal design scheme of uniform pressure surface welding magnet device, develops magnet devices with different structural sizes, builds an experimental platform for uniform pressure welding, realizes the high-quality welding of aluminum plate and stainless steel plate under different welding areas, and reveals the influence of welding process parameters and structural parameters on the welding quality and welding area of the joint. It provides a theoretical and experimental basis for increasing the welding area and improving the welding quality. The main results and conclusions are as follows:

1. The uniform pressure welding magnet device with different structural parameters is optimized and designed. By reducing the gap g between the coil and the conductive channel, the height h of the coil center, and the width w of the conductive channel opening, the magnetic pressure on the surface of the aluminum plate can be effectively increased; when the number of turns of the coil is $6 \sim 8$ and the outer radius is about 30 mm, the magnetic pressure on the surface of the plate is large and the welding effect is the best.
2. A high-performance magnet device with different structural parameters is developed, which realizes the high-quality surface welding of dissimilar metal plates with the length and width ranging from more than ten millimeters to tens of millimeters. Effective improvement methods are put forward for the problems of thinning tear and arc ablation at the chamfer of plates in uniform pressure welding.
3. The results show that increasing the discharge voltage can effectively increase the effective area of the welding area and improve the welding strength of the welded joint, but it will also aggravate the thinning of the chamfer; proper welding gap is helpful to increase the effective area of welding area and improve the tensile strength of welded joints; the length and width of the welding area can be effectively increased by increasing the opening width of the conductive channel and

the number of coil turns, which is helpful to realize the large-area welding of dissimilar metal plates.

Author contribution Hang Zhang: conceptualization, methodology, software, experiment and writing—original draft. Ning Liu, Xiaoxiang Li, and Qingjian Wang: software and auxiliary experiment. Hongfa Ding: supervision and review.

Availability of data and material Not applicable.

Code availability Not applicable.

Declarations

Ethical approval This study does not involve human participants or animals.

Consent to participate All the authors listed have approved to participate.

Consent for publication All the authors listed have been approved to publish in this journal.

Competing interests The authors declare no competing interests.

References

1. Qiu L, Li Y, Yu Y, Abu-Siada A, Xiong Q, Li X, Li L, Su P, Cao Q (2019) Electromagnetic force distribution and deformation homogeneity of electromagnetic tube expansion with a new concave coil structure. Ieee Access 7:117107–117114
2. Psyk V, Risch D, Kinsey BL, Tekkaya AE, Kleiner M (2011) Electromagnetic forming—a review. J Mater Process Tech 211:787–829
3. Qiu R, Iwamoto C, Satonaka S (2009) Interfacial microstructure and strength of steel/aluminum alloy joints welded by resistance spot welding with cover plate. J Mater Process Tech 209:4186–4193
4. Kapil A, Sharma A (2015) Magnetic pulse welding: an efficient and environmentally friendly multi-material joining technique. J Clean Prod 100:35–58
5. Kimchi M, Shao H, Cheng W, Krishnaswamy P (2004) Magnetic pulse welding aluminium tubes to steel bars. Weld World 48:19–22
6. Qiu L, Li Y, Yu Y, Xiao Y, Su P, Xiong Q, Jiang J, Li L (2019) Numerical and experimental investigation in electromagnetic tube expansion with axial compression. Int J Adv ManufTechnol 104:3045–3051
7. Manogaran AP, Manoharan P, Priem D, Marya S, Racineux G (2014) Magnetic pulse spot welding of bimetals. J Mater Process Tech 214:1236–1244
8. Miranda RM, Tomás B, Santos TG, Fernandes N (2014) Magnetic pulse welding on the cutting edge of industrial applications. Soldag Insp 19:69–81
9. Lueg-Althoff J, Bellmann J, Gies S, Schulze S, Tekkaya AE, Beyer E (2018) Influence of the flyer kinetics on magnetic pulse welding of tubes. J Mater Process Tech 262:189–203

10. Lueg-Althoff J, Bellmann J, Hahn M, Schulze S, Gies S, Tekkaya AE, Beyer E (2020) Joining dissimilar thin-walled tubes by magnetic pulse welding. J Mater Process Tech 279:116562

11. Faes K, Shotri R, De A (2020) Probing magnetic pulse welding of thin-walled tubes. J Manuf Mater Process 4(4):118

12. Aizawa T (2003) Magnetic pressure seam welding method for aluminium sheets. Weld Int 17:929–933

13. Aizawa T (2004) Magnetic-pressure seam welding methods of Al/Fe sheets. J Jpn Light Metal Weld 42

14. Weddeling C, Hahn M, Daehn GS, Tekkaya AE (2014) Uniform pressure electromagnetic actuator – an innovative tool for magnetic pulse welding. Procedia CIRP 18:156–161

15. Yu H, Tong Y (2017) Magnetic pulse welding of aluminum to steel using uniform pressure electromagnetic actuator. Int J Adv Manuf Technol 91:2257–2265

16. Kim JH, Kim D, Lee M (2015) Experimental and numerical analysis of a rectangular helical coil actuator for electromagnetic bulging. Int J Adv Manuf Technol 78:825–839